J Mater Sci (2007) 42:6316–6324
DOI 10.1007/s10853-006-1206-1

Sintering of an ultra pure α-alumina powder: I. Densification, grain growth and sintering path

Guillaume Bernard-Granger · Christian Guizard · Ahmed Addad

Received: 7 July 2006 / Accepted: 2 November 2006 / Published online: 22 April 2007

Abstract Sintering in air of an ultra pure α-alumina powder has been investigated. Isothermal experiments have been conducted on green samples shaped by slip casting. The grain growth and densification kinetics have been established. The ''relative density/grain size'' trajectory, called ''sintering path'', has been drawn. Hypotheses concerning the mechanisms controlling grain growth and densification have been formulated. For the first time, it is shown that grain growth and densification kinetics exhibit two distinct regimes, where an initial point defect formation step plays a key role. When point defects have been generated, the diffusion of the associated Al^{3+} cations controls grain growth and densification.

Introduction

Polycrystalline α-alumina is one of the most commonly used ceramic materials in the industrial world. It has several well-known key benefits: submicron raw powders are inexpensive relative to other fine ceramic materials; water based slurries are easily processed; various green shaping methods can be used; it sinters very well in air. When most of the porosity has disappeared, the obtained final room temperature properties of fired parts are very interesting. For example, Vickers hardness is higher than 20 GPa [1, 2]; fracture toughness is in the range 2.5–4.5 MPa $\sqrt{m}$ [3]; three point flexural strength is between 600 MPa and 850 MPa [1, 2]; it has a high resistance to diverse corrosive environments [4–6]; it exhibits an excellent wear resistance due to a low friction coefficient when alumina is in contact with alumina [3, 7, 8].

Polycrystalline α-alumina is also an interesting material because of its optical properties. In the early 60s, the now well-known commercial product Lucalox®, was discovered [9, 10]. It consists of a fully dense polycrystalline α-alumina, having an average grain size of some tens micrometers and free of any amorphous grain boundary phase. It has been used then as an excellent solution for envelopes for high-pressure sodium lamps.

The Lucalox® polycrystalline α-alumina is only a translucent material (not transparent) for visible, short range and mid-range infrared radiations [9–12]. It exhibits a very high total transmittance but only a poor in-line transmittance in the visible range (around 10% maximum for a sample thickness close to 1 mm [9, 11] and a wavelength of 0.5 μm) and a medium in-line transmittance in the mid-infrared range (around 66% maximum for a sample thickness of 1.2 mm and a wavelength of 5 μm [9]). Lucalox® has also low mechanical strength. Four-point flexural strength is reported to be between 330 MPa (grain size of 10 μm) and 170 MPa (grain size of 85 μm) [13].

More recently, it has been shown that fully dense polycrystalline α-alumina, with a submicron grain size, presents a high level of in-line transmittance in the visible range [1, 14]; this results may seem surprising because of the intrinsic birefringent nature of α-alumina single grains. But it has been also confirmed by a very nice theoretical

G. Bernard-Granger (✉) · C. Guizard
Laboratoire de Synthèse et Fonctionnalisation des Céramiques, FRE 2770 CNRS/Saint-Gobain, Saint-Gobain C.R.E.E., 84306 Cavaillon Cedex, France
e-mail: guillaume.bernard-granger@saint-gobain.com

A. Addad
Laboratoire de Structure et Propriétés de l'Etat Solide, UMR 8008 CNRS, Université des Sciences et Technologies de Lille, Bâtiment C6, 59655 Villeneuve d'Ascq Cedex, France

model developed recently by Apetz [11]. For example, Krell has obtained an in-line transmittance of 64% at a wavelength of 640 nm (laser red light), for a fully dense alumina sample (slightly doped with zirconia, grain size around 0.50 μm) having a thickness of 0.8 mm [2]. Krell has also clearly shown that fully dense polycrystalline α-alumina material, with a submicron grain size, is a transparent material similar to sapphire in the mid-infrared range (thickness of the analyzed samples around 1 mm, grain size of polycrystalline alumina in the range 0.50–0.70 μm) [11]. For this kind of submicron fully dense and ''transparent'' polycrystalline α-alumina, Krell has also observed, as mentioned previously, that the mechanical properties (especially flexural strength and hardness) are very good [1, 2].

The process developed by Krell to obtain green samples ready for sintering is based on the sol–gel technology [2, 14]. Since this method involves the use of monomers that are in most cases toxic and expensive, the authors believe that slip casting could be a better shaping method. This paper reports on the sintering behavior of an ultra pure alumina powder that is shaped by slip casting. The densification and grain growth kinetics in air are investigated and the natural sintering path is drawn. After a careful observation of the microstructure of fully dense samples having clearly a submicron grain size, the mechanisms controlling grain growth and densification are proposed.

The optical and mechanical properties, measured by Krell on the new generation of fully dense and submicron polycrystalline α-alumina, could be of a great interest for technical components that are exposed to severe conditions in service. Flat windows or missile domes, protecting infrared and visible detectors, are potential applications.

Experimental procedure

The TM-DAR raw powder (Taimei Chemicals Co. Ltd., Tokyo, Japan) is selected as the starting material. This powder is very pure; the main impurities, determined by inductively coupled plasma spectrometry or X-ray fluorescence, are 120 wt (weight) ppm of Na, 10 wt ppm of K, 10 wt ppm of Mg, 50 wt ppm of Si and 15 wt ppm of Ca. It is composed only of the α-alumina species (corundum structure, confirmed by X-ray diffraction) and has an average specific surface area around 13.5–14.0 m^2/g (determined using BET measurements). Scanning Electron Microscope (SEM) examinations show that this powder is constituted of more or less spherical aggregates having an average diameter between 5 μm and 50 μm. Each aggregate is composed of elemental more or less spherical crystallites having an average diameter between 100 nm and 150 nm, which is in good agreement with the specific surface area value mentioned above.

High-solids-loading (70 wt%), water based α-alumina slurries are prepared with the TM-DAR raw powder (ammonium polyacrylate and PEG20M are incorporated as a dispersant and as a binder, respectively). After deagglomeration, optimal blending and degassing, samples are slip cast in porous plaster molds. The diameter of the samples for sintering runs is typically 40 mm in diameter and 4 mm in thickness. The average relative green density is around 63%.

When setting is completed, the green samples are put in a drying oven for a period of some hours. After a debindering step in air (480 °C/3 h), the samples are then ready for the sintering experiments.

To identify the sintering window of interest, vertical dilatometer tests are completed. Different heating rates are selected: 100, 300 and 650 °C/h. The results obtained are visible in Figs. 1 and 2. It appears that linear shrinkage ($\Delta L/L_0$), and consequently densification, is the most pronounced when the heating rate is 100 °C/h (Fig. 1). When the heating rate is 100 °C/h, the linear shrinkage rate ($d(\Delta L/L_0)/dt$) is maximal when the temperature reaches 1,252 °C. Furthermore, it also appears that the linear shrinkage rate is maximum for a lower temperature in comparison to what is obtained with the other heating rate values (1,263 °C and 1,288 °C for 300 °C/h and 650 °C/h, respectively). It has been arbitrary decided to use in all cases a heating rate fixed to 100 °C/h and to retain the following three temperatures for our sintering experiments: 1,218 °C (peak temperature minus 34 °C), 1,252 °C (peak temperature), 1,287 °C (peak temperature plus 35 °C). Concerning the soak time at each temperature, it is in the range 0–6 h.

The different isothermal sintering runs constituting the experimental matrix are conducted in air, in a standard electrical furnace equipped with Kanthal (a FeCrAlCo

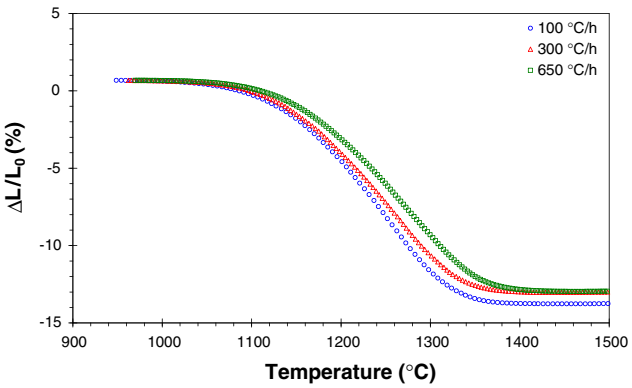

Fig. 1 Vertical dilatometer experiments performed with different heating rates

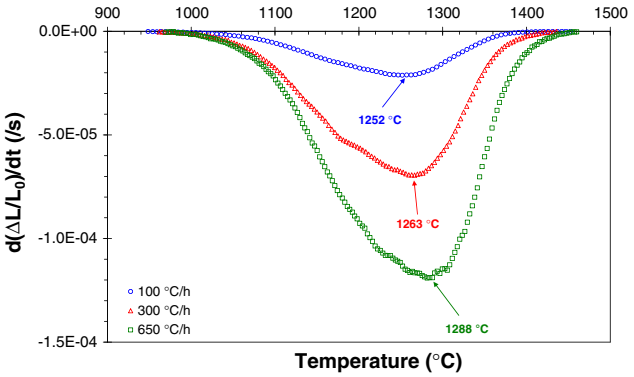

Fig. 2 Shrinkage rate obtained from vertical dilatometer experiments

alloy) heating elements. For each run, at least 10 samples are sintered at the same time. The sintering furnace cycle involves heating up at 100 °C/min, holding at the soak temperature and free cooling to room temperature.

The apparent volume mass of the sintered samples is measured using the Archimedes method with deionized water (three measurements were made for each sample). Then, the relative density, D, is obtained using a theoretical volume mass of alumina of 3.976 g/cc (calculated from the elemental lattice structure of the α-alumina phase).

The as-sintered microstructure is characterized by observing fractured surfaces using SEM. The average grain size, G, is measured from SEM pictures, using a line-intercept method taking into account at least 300 grains. A three-dimensional correction factor of 1.2 has been used. So, it means that the individual grains are approximated by spheres. Such an approximation is useful when theoretical calculations are performed to evaluate the real in-line transmittance of a polycrystalline window [11]. A typical post-sintering microstructure obtained from fracture surfaces is shown on Fig. 3.

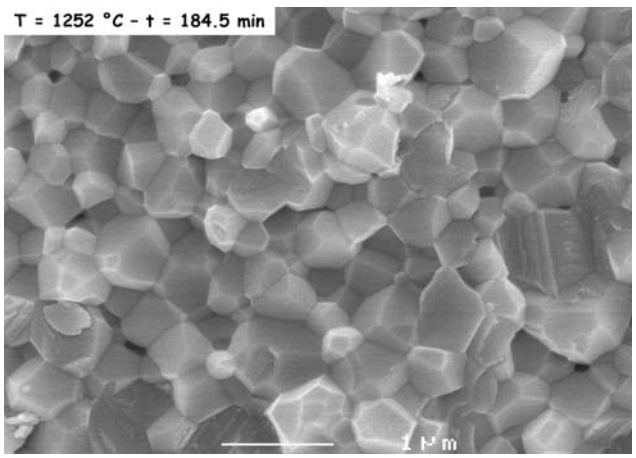

Fig. 3 Isothermal sintering—Typical as-sintered microstructure

To propose realistic mechanisms controlling grain growth and densification, it is important to observe carefully the microstructure of the sintered material. That is why transmission electron microscopy (TEM) has been conducted on fully dense sintered samples (additional HIP treatment after sintering). For that, thin foils have been prepared by mechanical polishing followed by ion milling. The foils have been covered with a thin layer of graphite and have been observed using a Philips CM30 microscope (Philips Research Laboratories, Eindhoven, The Netherlands, acceleration voltage of 300 kV, point to point resolution of 0.19 nm) equipped with an EDS (Energy Dispersive Spectroscopy) microanalysis system (Thermo Electron Corporation, Waltham, MA, USA, Noran system equipped with an ultra-thin window). The general microstructure is observed in the bright field mode. Local EDS analyses are performed using the Scanning Transmission Electron Microscopy (STEM) mode in the elemental alumina grains, at the grain boundaries and at triple points using a probe size of 5.6 nm. Quantitative analyses are carried out using the Doukhan-Van Cappellen method, based on electro-neutrality of the specimen, to have access to the local thin foil thickness [15]. Some additional investigations are also done using the High Resolution Transmission Electron Microscopy (HRTEM) mode, especially at the grain boundaries.

Experimental results

Grain growth and densification kinetics

Figures 4 and 5, respectively, show how grain growth and densification progress as a function of the soak time at high temperature.

Whatever is the sintering temperature, grain growth appears to be very rapid at the beginning and slows down after a certain period of time (around 100 min). Quite

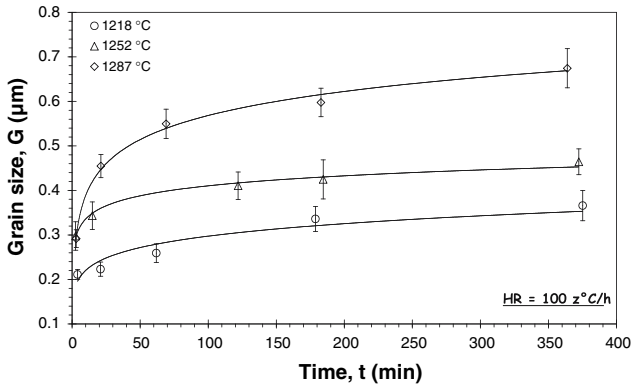

Fig. 4 Isothermal sintering—Grain growth kinetic

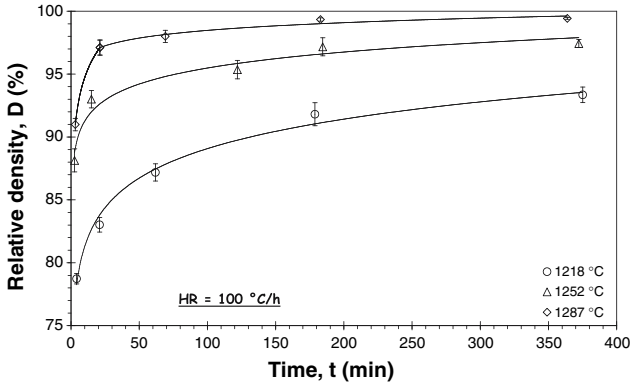

Fig. 5 Isothermal sintering—Densification kinetic

often, it is advanced that such a decaying grain growth is due to the build-up of impurity concentrations at grain boundaries [16, 17].

Concerning the evolution of the relative density as a function of time, it appears that the higher the soak temperature, the greater is the densification during the heating ramp step. For example, for the samples sintered at 1,287 °C, a condition of closed porosity (D > 90–92%) is achieved before reaching the soak temperature. In that case, it signifies that most of the densification takes place under non-isothermal conditions.

Figure 6 shows the ''grain size/relative density'' trajectory, called ''sintering path'', for green samples obtained by slip casting and sintered in air at high temperature. It is interesting to note that all the experimental points fall on the same curve (doted line on Fig. 6). It means that a multitude of sintering couples ''temperature/soak time'' will yield the same sintered microstructure. Furthermore, it appears that it is possible to obtain sintered samples with a relative density higher than 92% (i.e. porosity is totally closed) and a grain size well below 0.5 μm. Finally, it seems impossible to obtain fully dense samples with a grain size well below 1 μm. This

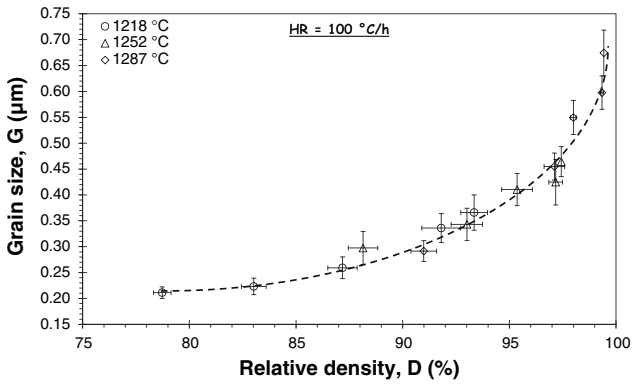

Fig. 6 Isothermal sintering—Sintering path

observation is similar to what is observed during sintering of pure alumina with coarser raw powders [18, 19]. Contrary to what one might think, decreasing as much as possible the starting grain size of the raw powder is not an effective solution to obtain fully dense samples in one pressureless sintering step.

At this point, it is important to mention that Chen [20, 21] and Binner [22] have developed a 2-stage sintering process, which enables to maintain a very fine microstructure in the final samples. But, the materials they obtained are not ''really'' fully dense. Firstly, Chen does not mention the fact that his Y_2O_3 samples are transparent/translucent in the visible range. Secondly, he speaks only about samples ''near full density''. Then, it is suspected that a tiny residual porosity, which is impossible to quantify using standard methods as the Archimedes one, remain. Binner clearly says that his zirconia samples have a relative density around 99.4%. So, to obtain fully dense material, both investigators will also need a pressure assisted post treatment, as we have done (section ''Microstructure observed in fully dense samples''). That is why, at this point, we do not see any real advantage of such a 2-step sintering process for the production of ''real'' fully dense materials. Of course, it is not true anymore if a tiny residual porosity is accepted in the final material.

Microstructure observed in fully dense samples

A complementary HIP step was performed on samples sintered at 1,252 °C during 3 h (D = 97.2%, G = 0.43 μm). It consisted in applying to the samples an argon pressure of 200 MPa during 15 h at a temperature of 1,200 °C. If the pressureless sintered samples were opaque with a white color, they became translucent and slightly gray after HIPping. All the samples were measured to be fully dense after HIPping.

Figure 7a show the typical microstructure observed by TEM for the HIPed samples.

All the elemental grains have an equiaxial shape. No extensive abnormal grain growth is observed, even if locally some grains, larger than the average grain size, may be seen. The average grain size is measured to be 0.55 ± 0.06 μm. In comparison to the as-sintered value, an increase of 27.9% of the average grain size is attributable to the HIP step treatment. It signifies to the authors that the HIP conditions were not optimal since they aimed to limit as much as possible grain growth during this step. Recently, more improved HIP conditions have been identified from compressive creep experiments on the as-sintered samples [23].

Despite the relative density measured experimentally to be 100 %, some residual intragranular pores are occasionally observed as shown on Fig. 7b (see arrows). They

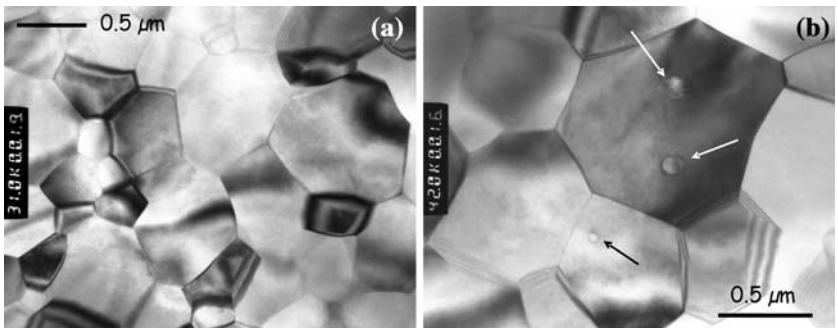

Fig. 7 Typical microstructure after HIP

are homogeneously distributed in all the thin foil and they do not segregate to form locally large defects. The presence of these few trapped pores signifies that the sintering path obtained in this study is close to the boundary/pores separation limit.

Chemical analyses performed on HIPed samples are summarized in Table 1. In contrast to the impurity contents measured on the raw powder (see section ''Experimental procedure'') it appears that a strong enrichment in SiO_2 and CaO takes place during the sample preparation described in this article. At this point, the authors believe that casting in a plaster mold is responsible for the significant increase in the CaO content. As for SiO_2, the authors think that the increase in concentration is coming from the alumina grinding media that was used.

Using HRTEM, grain boundaries and triple points appear to be free of any amorphous phase. Local EDS analyses performed in the center of the elemental grains, at grain boundaries and at triple points appear to be very interesting (Fig. 8). Some grains appear to be substituted in Si, Ca and/or K (Fig. 8b, average standard deviation of the different concentrations is between ±0.01 and ±0.04 wt%). All the grain boundaries analyzed exhibit at least Si and in most cases also Ca and K (Fig. 8c, average standard deviation of the different concentrations is between ±0.01 and ±0.04 wt%). Finally, the triple points appear to be clearly enriched in Si, Ca and K (Fig. 8d, average standard deviation of the different concentrations is also between ±0.01 and ±0.04 wt%).

One comment about the Ca concentration in some alumina grains may be added. Bae [24] has proposed that the solubility limit of CaO in alumina is around 30 wt ppm. So it is much lower that what is occasionally measured in some of our alumina grains (between 200 wt ppm and 700 wt ppm). At this time, we have no clear explanation for such an observation. It could be advanced that the nature of the core of the starting elemental crystallites in the raw powder is something else than pure α-alumina. TEM observations coupled with nano EDS analyses will be performed on the raw powder, in the future, to confirm/invalidate this hypothesis.

Table 1 Impurity contents after HIP

SiO_2	CaO	MgO	Na_2O	K_2O
410	220	40	150	8

Concentrations are in weight ppm

Discussion

From EDS analyses performed at grain boundaries and at triple points it is evident that Si, Ca and K segregate to these locations. If HRTEM does not show any amorphous intergranular thin film or amorphous triple point, one can think about bad orientation conditions during these observations (grain boundaries analyzed not scrupulously edge-on, special grain boundaries in perfect conditions of coincidence...). This argument can be refuted by a simple consideration.

Clarke has shown that the equilibrium thickness of an amorphous silica film between two alumina grains is around 2 nm [25]. If such an amorphous thin film is present at all grain boundaries, it is possible to calculate what is the minimal volume fraction of glassy phase, V_g^m, present in such a material having an average grain size G. Assuming, for this calculation, that the grain shape is a tetrakaidecahedron (truncated octahedron), it is possible to establish the minimal volume fraction of glass as follows:

$$V_g^m = \frac{S_t}{V_t}\frac{h_0}{2} = \frac{12\sqrt{3}+6}{8}\frac{h_0}{G} \quad (1)$$

where S_t and V_t are, respectively, the surface and the volume of a tetrakaidecahedron and have been expressed by Zhao as a function of the average grain size G [26]. Assuming a film thickness of 2 nm and an average grain size of 0.55 μm (obtained using a sphere approximation, but it will be the worst cases because the three-dimensional factor of 1.2 is the smallest one for such a geometry) in the fully dense samples (see section ''Microstructure observed in fully dense samples''), the minimal volume fraction of amorphous phase necessary to wet all grain boundaries is

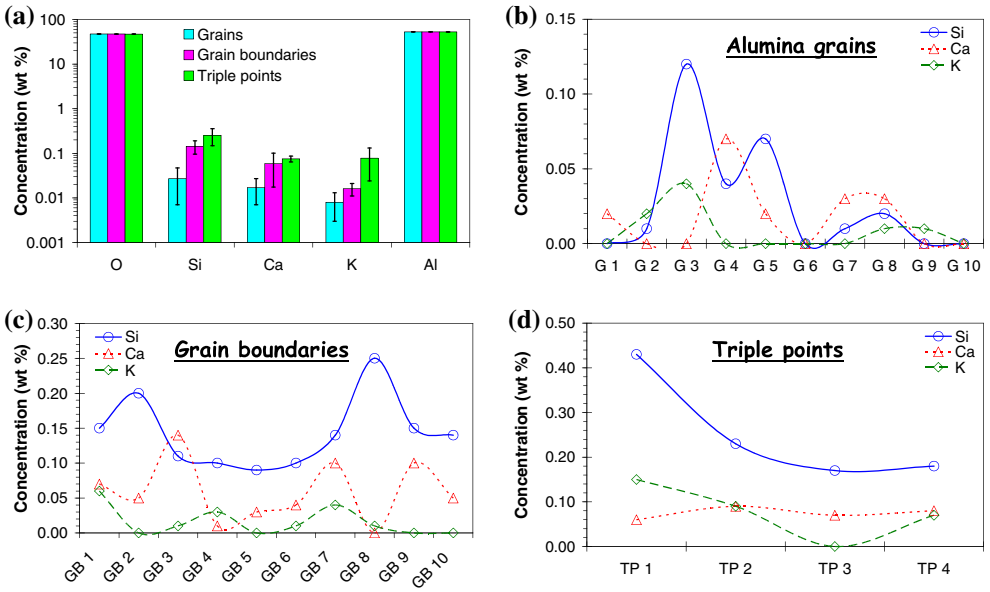

Fig. 8 STEM analyses—Spot size = 5.6 nm

then calculated to be 1.2%. Chemical analyses measured after HIP (Table 1) have shown that the total amount of silica impurity is 410 ppm in weight which corresponds roughly to 0.07% in volume. This amount is clearly well below the minimal volume fraction that is essential to wet all grain boundaries. A more precise calculation could be done by assuming that, in alumina, the intergranular glassy phase is more an aluminosilicate glass than pure silica. In that case, the total glass content would be higher than 0.07 vol%, but definitely lower than the 1.2 vol% required to form a continuous grain boundary film of equilibrium thickness. Therefore, the lack of intergranular amorphous film noticed in the fully dense samples by HRTEM is justified. Consequently, it signifies that all the impurities are concentrated near the grain boundaries by the way of a solute segregation as it has been also observed by Li in alumina [27].

To identify the mechanism controlling grain growth, it is common to use the well-known relation [28, 29]:

$$G^m = Kt + G_0^m \tag{2}$$

where K is a rate constant depending on the mechanism controlling grain growth, t is time, G_0 is the initial grain size (t = 0, no soak, just the heating step) and m is an exponent characteristic of the grain growth mechanism.

If two different grain growth regimes are considered, it is for a m value of 2 that the fit of the experimental data is the best, as it can be seen on Fig. 9. This m value is consistent with grain growth being controlled by the grain boundaries and the motion of the grain boundaries being themselves controlled by a weak solute (Si, Ca and Al) drag mechanism (high solubility of impurities in the alumina grains in the vicinity of grain boundaries) [30]. This assumption is in very good agreement with the EDS measurements performed at grain boundaries and at triple points in the fully dense samples.

To be able to have access to the apparent activation energy of the mechanism controlling grain growth, relation (2) can be modified as follows:

$$RTK = K_0 e^{-\frac{Q_{gg}}{RT}} \tag{3}$$

where R is the universal gas constant, T is the absolute temperature, K_0 is a constant and Q_{gg} is the apparent activation energy of the mechanism controlling grain growth. Using relation (3) in the logarithmic form and with a value of m of 2, it is possible to calculate two different values for Q_{gg} corresponding to the two grain growth regimes, as it is shown on Fig. 10. For the first regime (t = 10 min), the apparent activation energy for grain growth is around 810 kJ/mol. For the second regime

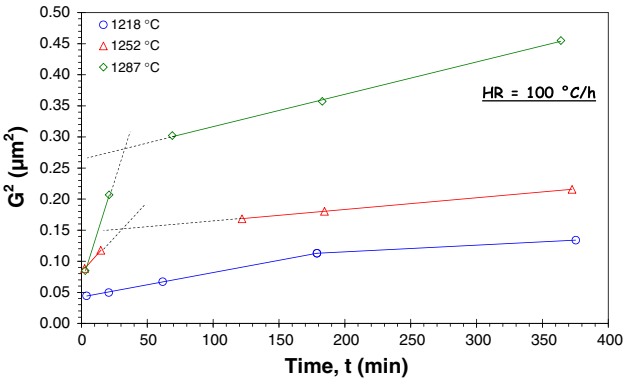

Fig. 9 Isothermal sintering—Mechanism controlling grain growth

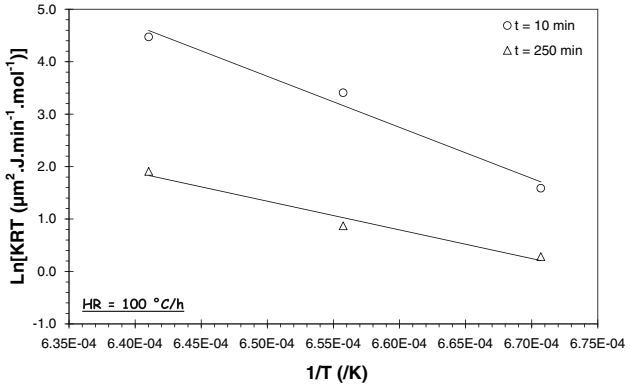

Fig. 10 Isothermal sintering—Activation energy for grain growth

(t = 250 min), the apparent activation energy for grain growth is calculated to be close to 455 kJ/mol.

Most of the time it is not easy to identify what mechanism is really controlling grain growth, densification or creep in polycrystals. But at least, some propositions may be advanced. El-Aiat has shown that the Frenkel disorder (equilibrium constant is $K_F = [V_{Al}'''][Al_i^{\circ\circ\circ}]$ using the Kröger–Vink formalism) energy of formation in alumina is roughly 790 kJ/mol [31]. It has been also shown that the activation energy for the bulk diffusion of Al^{3+} in alumina is between 477 kJ/mol and 510 kJ/mol [32, 33].

Therefore, we propose that grain growth in the first regime is controlled by the formation of Frenkel defects. This leads to the fast grain growth observed for the short soak durations whatever is the sintering temperature. Then, grain growth in the second regime would be controlled by the diffusion of the atoms associated to the Frenkel disorders through grain boundaries and more especially by the diffusion of the Al^{3+} cations. The results presented here imply that grain boundaries, and the solute segregation (Si, Ca and K) which takes place to these locations, do not have a strong influence on the migration of Al^{3+} cations; the apparent activation energy measured in the second phase of grain growth is similar to the one of the Al^{3+} cations in the bulk of sapphire.

For identification of the mechanism controlling densification, the following relation is employed [34]:

$$\frac{1}{D}\frac{dD}{dt} = \frac{K}{G^n} \tag{4}$$

where $\frac{dD}{dt}$ is the densification rate, K is a rate constant depending on the mechanism controlling densification and n is an exponent characteristic of the densification mechanism. When densification is controlled by volume diffusion, n has a value of 3. When densification is controlled by grain boundary diffusion, the value of n is 4.

When one considers all three sintering temperatures and two regimes at each temperature, one sees that an exponent 4 gives a good fit to the experimental data (Fig. 11). This signifies that densification in the sintered alumina samples proceeds via grain boundary diffusion, the solute segregation (Si, Ca and K) in the vicinity of grain boundaries having a marginal influence on it. The difference between the first and second regimes may be linked to the step controlling grain boundary diffusion.

Knowing that n is equal to 4, it is possible to modify relation (4) to have access to the apparent activation energy of the mechanism controlling densification:

$$\frac{dD}{dt} = \frac{K_1}{RTG^4} e^{-\frac{Q_d}{RT}} \tag{5}$$

where K_1 is a constant for a fixed relative density value, R is the universal gas constant, T is the absolute temperature and Q_d is the apparent activation energy of the mechanism controlling densification. Using relation (5) in the logarithmic form and using a constant relative density value of 93% (this is roughly the only one which is common for the three sintering temperatures used, see Fig. 5), it is possible to obtain one apparent activation energy for the mechanism controlling densification when the porosity is closed, as it is shown on Fig. 12. In that case, the apparent activation energy obtained is around 1,150 kJ/mol. Such a value is similar to what has been reported in other recent investigations on sintering of very fine alumina powders [35, 36].

Another technique of interest to determine the apparent activation energy for densification is the Constant Rate of Heating (CRH) one [37–39]. Using the vertical dilatometer tests performed to identify the sintering window (see section ''Experimental procedure'') and the formalism of the CRH method, it is possible to obtain the instantaneous apparent activation energy controlling densification, for different values of shrinkage corresponding to a residual porosity still opened. The result can be seen of Fig. 13. The average value obtained is 1,040 ± 50 kJ/mol. This value is in very good agreement with the one obtained

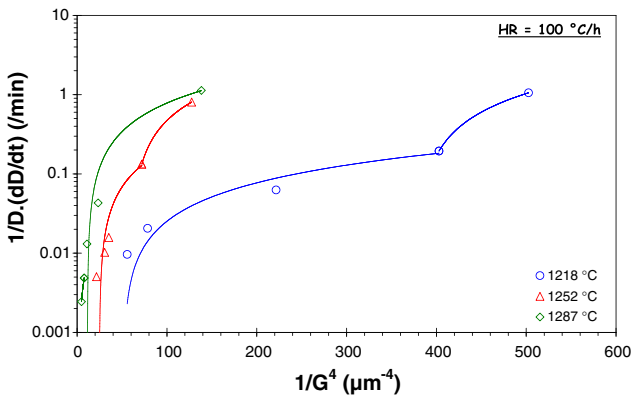

Fig. 11 Isothermal sintering—Mechanism controlling densification

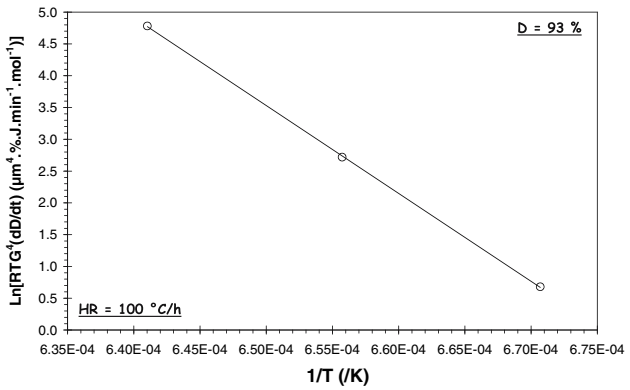

Fig. 12 Isothermal sintering—Activation energy for densification

previously from the isothermal sintering experiments when the residual porosity is closed. It is concluded that the apparent activation energy of the mechanism controlling the densification of the alumina samples is 1,095 ± 55 kJ/mol, whatever is the instantaneous relative density of the sample.

During densification, the displacements of alumina and oxygen vacancies are both of great importance. In that case, it is thought that the role devoted to Schottky disorders (equilibrium constant is $K_S = [V_{Al}'''']^2[V_O^{\circ\circ}]^3$ using the Kröger–Vink formalism) is critical. El-Aiat has also shown that the Schottky disorder energy of formation in alumina is roughly 630 kJ/mol [31]. It has also been shown that the activation energy for the grain boundary diffusion of Al^{3+} in alumina is 420 kJ/mol [33].

Therefore, we propose that densification is controlled by the formation of Schottky disorders and by the diffusion of the atoms associated to the Schottky disorders, the grain boundary diffusion of the Al^{3+} cations being the limiting step. The total apparent activation of such a mechanism is 1,050 kJ/mol (630 + 420 kJ/mol), which is not too far from 1,095 kJ/mol, the average experimental value we obtained.

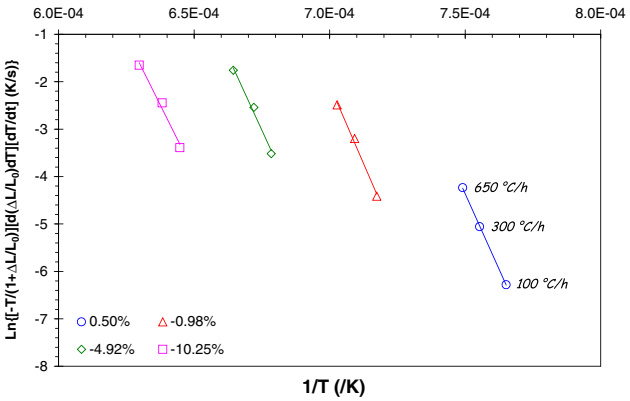

Fig. 13 Activation energy for densification obtained with the CRH method

Conclusion

Sintering in air of an ultra pure α-alumina powder has been investigated. Green samples have been obtained by slip casting. Isothermal experiments have been conducted with a heating rate of 100 °C/h, at temperatures around the one corresponding to the maximal linear shrinkage rate observed during vertical dilatometer tests performed with the same heating rate. The grain growth and densification kinetics have been established. The ''grain size/relative density'' trajectory, called ''sintering path'', has been finally drawn.

Grain growth and densification kinetics exhibit two distinct regimes. The authors propose that grain growth in the first regime is controlled by a Frenkel disorders formation step. Grain growth in the second regime would be controlled by the diffusion of the atoms associated to the Frenkel disorders through grain boundaries and more especially by the diffusion of the Al^{3+} cations. Secondly, the authors propose that densification is controlled by the formation of Schottky disorders and by the diffusion of the atoms associated to the Schottky disorders, the grain boundary diffusion of the Al^{3+} cations being the limiting step.

In a companion paper, we will focus on the mechanical, thermomechanical and optical properties (in the UV, visible and infrared ranges) of such a polycrystalline alumina material, brought to full density by a complementary HIP treatment (G. Bernard-Granger and C. Guizard, to be submitted).

References

1. Krell A, Blank P, Ma H, Hutzler T, Nebelung M (2003) J Amer Ceram Soc 86(4):546
2. Krell A, Blank P, Ma H, Hutzler T, van Bruggen MPB, Apetz R (2003) J Amer Ceram Soc 86(1):12
3. Munro RG (1997) J Amer Ceram Soc 80(8):1919
4. Schacht M, Boukis N, Dinjus E (2000) J Mater Sci 35(24):6251, DOI: 10.1023/A:1026714218522
5. Mikeska KR, Bennison SJ (1999) J Amer Ceram Soc 82(12):3561
6. Oda K, Yoshio T (1997) J Amer Ceram Soc 80(12):3233
7. Dogan CP, Hawk JA (1999) Wear 225–229(2):1050
8. Kalin M, Novak S, Vizintin J (2003) Wear 254(11):1141
9. Coble RL (1962) U.S. Patent 3,026,210
10. St. Pierre PDS, Gatti A (1962) U.S. Patent 3,026,177
11. Apetz R, van Bruggen MPB (2003) J Amer Ceram Soc 86(3):480
12. Wei GC, Hecker A, Goodman DA (2001) J Amer Ceram Soc 84(12):2853
13. Gupta TK (1972) J Amer Ceram Soc 55(5):249
14. Krell A, Baur G, Dähne C (2003) Proc SPIE 5078:199
15. Van Cappellen E, Doukhan JC (1994) Ultramicroscopy 53:343

16. Voytovych R, Mac Laren I, Gülgun MA, Cannon RM, Rühle M (2002) Acta Mater 50:3453
17. Cahn JW (1962) Acta Metal 10:789
18. Berry KA, Harmer MP (1986) J Amer Ceram Soc 69(2):143
19. Thompson AM, Harmer MP (1993) J Amer Ceram Soc 76(9):2248
20. Wang X-H, Chen P-L, Chen I-W (2006) J Amer Ceram Soc 89(2):431
21. Chen IW, Wang XH (2000) Nature 404:168
22. Binner J (2006) Processing Nanostructured Structural Ceramics. Informal communication
23. Bernard-Granger G, Guizard C, Duclos R (2006) J Mater Sci, doi:10.1007/s10853-006-1379-7
24. Bae S, Baik S (1993) J Amer Ceram Soc 76(4):1065
25. Clarke DR (1987) J Amer Ceram Soc 70(1):15
26. Zhao J, Harmer MP (1988) J Amer Ceram Soc 71(2):113
27. Li C-W, Kingery WD (1984) Adv Ceram 10:368
28. Gruffel P, Carry CP (1993) J Eur Ceram Soc 11:189
29. Loudjani MK, Cortes R (2000) J Eur Ceram Soc 20:1483
30. Brook RJ (1968) Scripta Met 2:375
31. El-Aiat MM, Kröger FA (1982) J Amer Ceram Soc 65(3):162
32. Le Gall M, Lesage B, Bernardi J (1994) Phil Mag A 70(5):761
33. Frost HJ, Ashby MF (2001) Deformation-mechanism maps: the plasticity and creep of metals and ceramics. Web version, Chapter 14
34. Su H, Johnson DL (1996) J Amer Ceram Soc 79(12):3211
35. Lance D (2004) Frittage de l'Alumine α Submicronique. Nouvelle Relation Dilatométrie / Evolution Microstructurale. Ph.D. Thesis in Materials Science, Saint-Etienne School of Mines and Jean Monnet University
36. Fang T-T, Shiue J-T, Shiau F-S (2003) Mater Chem Phys 80:108
37. Sato E, Carry CP (1995) J Eur Ceram Soc 15:9
38. Sato E, Carry CP (1996) J Amer Ceram Soc 79(8):2156
39. Matsui K, Ohmichi N, Ohgai M (2005) J Amer Ceram Soc, DOI: 10.1111/j.1551-2916.2005.00620.x